





# Selective electrooxidation of 2-propanol on Pt nanoparticles supported on $\text{Co}_3\text{O}_4$ : an *in-situ* study on atomically defined model systems

Tian Yang<sup>1,2,6</sup>, Maximilian Kastenmeier<sup>2</sup>, Michal Ronovsky<sup>3</sup>, Lukáš Fusek<sup>3</sup>, Tomáš Skála<sup>3</sup> , Fabian Waidhas<sup>2</sup>, Manon Bertram<sup>2</sup>, Nataliya Tsud<sup>3</sup>, Peter Matvija<sup>3</sup>, Kevin C Prince<sup>4</sup> , Vladimír Matolín<sup>3</sup>, Zhi Liu<sup>1,5</sup>, Viktor Johánek<sup>3</sup> , Josef Mysliveček<sup>3</sup> , Yaroslava Lykhach<sup>2</sup>, Olaf Brummel<sup>2</sup>  and Jörg Libuda<sup>2</sup>

<sup>1</sup> State Key Laboratory of Functional Materials for Informatics, Shanghai Institute of Microsystem and Information Technology, Chinese Academy of Sciences, Shanghai 200050, People's Republic of China

<sup>2</sup> Interface Research and Catalysis, ECRC, Friedrich-Alexander-Universität Erlangen-Nürnberg, Egerlandstr. 3, D-91058 Erlangen, Germany

<sup>3</sup> Faculty of Mathematics and Physics, Department of Surface and Plasma Science, Charles University, V Holešovičkách 2, Prague 18000, Czech Republic

<sup>4</sup> Elettra-Sincrotrone Trieste SCpA, Strada Statale 14, km 163.5, Basovizza-Trieste 34149, Italy

<sup>5</sup> School of Physical Science and Technology, ShanghaiTech University, Shanghai 201210, People's Republic of China

<sup>6</sup> University of Chinese Academy of Sciences, Beijing 100049, People's Republic of China

E-mail: [olaf.brummel@fau.de](mailto:olaf.brummel@fau.de)

Received 9 October 2020, revised 18 December 2020

Accepted for publication 8 January 2021

Published 4 February 2021



CrossMark

## Abstract

2-Propanol and its dehydrogenated counterpart acetone can be used as a rechargeable electrofuel. The concept involves selective oxidation of 2-propanol to acetone in a fuel cell coupled with reverse catalytic hydrogenation of acetone to 2-propanol in a closed cycle. We studied electrocatalytic oxidation of 2-propanol on complex model Pt/ $\text{Co}_3\text{O}_4$ (111) electrocatalysts prepared in ultra-high vacuum and characterized by scanning tunneling microscopy. The electrocatalytic behavior of the model electrocatalysts has been investigated in alkaline media (pH 10, phosphate buffer) by means of electrochemical infrared reflection absorption spectroscopy and *ex-situ* emersion synchrotron radiation photoelectron spectroscopy as a function of Pt particle size and compared with the electrocatalytic behavior of Pt(111) and pristine  $\text{Co}_3\text{O}_4$ (111) electrodes under similar conditions. We found that the  $\text{Co}_3\text{O}_4$ (111) film is inactive towards electrochemical oxidation of 2-propanol under the electrochemical conditions (0.3–1.1  $V_{\text{RHE}}$ ). The electrochemical oxidation of 2-propanol readily occurs on Pt(111) yielding acetone at an onset potential of 0.4  $V_{\text{RHE}}$ . The reaction pathway does not involve CO but yields strongly adsorbed acetone species leading to a partial poisoning of the surface sites. On model Pt/ $\text{Co}_3\text{O}_4$ (111) electrocatalysts, we observed distinct metal support interactions and particle size effects associated with the charge transfer at the metal/oxide interface. We found that ultra-small



Original content from this work may be used under the terms of the [Creative Commons Attribution 4.0 licence](https://creativecommons.org/licenses/by/4.0/). Any further distribution of this work must maintain attribution to the author(s) and the title of the work, journal citation and DOI.

Pt particles (around 1 nm and below) consist of partially oxidized  $\text{Pt}^{\delta+}$  species which show minor activity towards 2-propanol oxidation. In contrast, conventional Pt particles (particle size of a few nm) are mainly metallic and show high activity toward 2-propanol oxidation.

Supplementary material for this article is available [online](#)

Keywords: isopropanol, isopropyl alcohol, platinum, cobalt oxide, model electrocatalysts

(Some figures may appear in colour only in the online journal)

## 1. Introduction

The temporal fluctuations in the availability of renewable energies require the development of efficient energy storage systems. One of the most commonly discussed means of energy storage is hydrogen. However, hydrogen storage and distribution typically demands high pressures or low temperatures and, as a result, a very specific infrastructure [1, 2]. Alternative concepts for hydrogen storage are rechargeable fuels like, e.g. liquid organic hydrogen carriers (LOHCs), which are compatible with the common infrastructure for the distribution of liquid fuels [3, 4]. In LOHCs, hydrogen is reversibly bound to an organic carrier molecule like N-ethylcarbazole [3, 5–8] or Malotherm and catalytically released when required [9].

Recently, 2-propanol/acetone came into focus as a reversible LOHC couple because 2-propanol can be fed straight into a direct alcohol fuel cell yielding acetone as a product [10–15]. While the 2-propanol/acetone couple has a relatively low hydrogen storage capacity, successful strategies were devised which employ the 2-propanol/acetone couple in combination with classical LOHCs [10]. In the combined concept, long-term storage is established using the LOHC Malotherm, providing high hydrogen storage capacity. In a closed cycle, stored hydrogen is then transferred to acetone yielding 2-propanol, which is used as rechargeable fuel in the fuel cell. Thus, we avoid any molecular hydrogen in the system and increase the efficiency of energy conversion from LOHC-bound hydrogen to electricity from less than 38% for conventional LOHC concepts to over 50% [10].

2-Propanol is converted to acetone selectively both in acidic [16–18] and alkaline environments [19, 20]. In alkaline environment, noble metal particles supported by transition metal oxides like  $\text{CeO}_2$  and  $\text{Co}_3\text{O}_4$  showed improved performance in alcohol oxidation [21, 22]. The surface chemistry of such oxide supported catalysts is quite complex and, therefore, well-defined model systems are required for an atomistic understanding of the support effects [23]. In heterogeneous catalysis, the model catalysis approach contributed essentially to the current level of knowledge of supported catalysts [24]. In this approach, metal nanoparticles (NPs) are prepared on atomically defined oxide surfaces and studied by surface science methods. Here, we use the same approach to study an electrocatalytic reaction.

Specifically, we prepared  $\text{Co}_3\text{O}_4(111)$  surfaces on Ir(100) and deposited Pt NPs on this support in ultra-high vacuum (UHV). Previously we showed that the surface structure of this model catalyst is preserved upon transfer into the

electrochemical environment and in an alkaline environment within the determined stability window (0.3–1.1  $V_{\text{RHE}}$  at pH 10) [25–27]. Furthermore, we studied particle size effects [25, 28], electronic metal–support interactions (EMSI) [25, 27, 29], and investigated how these effects affect the stability of the model electrocatalysts [26]. Specifically, we showed that partially oxidized  $\text{Pt}^{\delta+}$  is formed at the interface between the NPs and the oxide support. For larger Pt NPs in the nm-size range, metallic  $\text{Pt}^0$  is the dominating species and the  $\text{Pt}^{\delta+}$  species are located at the metal–support interface only. In sharp contrast, ultrasmall particles of 1 nm and below show a very different electronic structure, i.e. they comprise of  $\text{Pt}^{\delta+}$  species only. Interestingly, the  $\text{Pt}^{\delta+}$  can stabilize particles against sintering and dissolution [26, 27, 30], and opens new reaction pathways for the CO oxidation by activation of oxygen from the support [26, 29].

While we only investigated the CO oxidation on  $\text{Pt}/\text{Co}_3\text{O}_4(111)$  in previous studies, here we focus on a more complex reaction, i.e. the 2-propanol electrooxidation. We prepared Pt particles of different size, characterized the samples by scanning tunneling microscopy (STM) and studied the 2-propanol oxidation by ex-situ emersion synchrotron radiation photoelectron spectroscopy (SR-PES) and electrochemical infrared (IR) reflection absorption spectroscopy (EC-IRRAS). We demonstrate that  $\text{Pt}/\text{Co}_3\text{O}_4$  catalysts can be highly active and selective for the electrooxidation of 2-propanol. However, the Pt particle size strongly affects the activity of the catalyst.

## 2. Methods

### 2.1. Sample preparation

The  $\text{Co}_3\text{O}_4(111)$  and  $\text{Pt}/\text{Co}_3\text{O}_4(111)$  samples employed in EC-IRRAS experiments were prepared and characterized in an UHV chamber at the Friedrich-Alexander-Universität Erlangen-Nürnberg, Germany. The setup was equipped with a dedicated transfer system enabling the transfer of the sample from UHV into the electrochemical environment without exposure to ambient conditions. For a detailed description of the setup we refer to the literature [31]. Briefly, the system comprises a low energy electron diffraction (LEED) optics, a quartz crystal microbalance (QCM), an ion gun, electron beam evaporators, a gas dosing system, and a transfer stage.  $\text{Co}_3\text{O}_4(111)$  and  $\text{Pt}/\text{Co}_3\text{O}_4(111)$  samples for STM characterization were prepared and characterized in a similarly equipped UHV setup at Charles University in Prague (CUP) containing, in addition, a laboratory x-ray photoelectron spectrometer and

a homemade STM. The samples used for SR-PES were prepared and analyzed at the Materials Science Beamline (MSB) of the Elettra Synchrotron in Trieste, Italy.

**2.1.1. Preparation of  $\text{Co}_3\text{O}_4(111)$  and  $\text{Pt}/\text{Co}_3\text{O}_4(111)$ .** Well-ordered  $\text{Co}_3\text{O}_4(111)$  films were prepared on the Ir(100) substrate following the procedure described by Heinz, Hammer and coworkers [32, 33]. We slightly adapted the procedure to different UHV preparation systems. The following procedure describes the preparation of samples used for EC-IRRAS measurements. The Ir(100) single crystal (MaTecK, 99.99%, depth of roughness  $<0.01 \mu\text{m}$ , accuracy of orientation  $<0.1^\circ$ ) was cleaned by several cycles of  $\text{Ar}^+$  sputtering (Linde 6.0,  $1 \times 10^{-4}$  mbar, 1.8 keV, 300 K), followed by annealing in UHV (1073 K, 10 min) and in  $\text{O}_2$  (Linde 5.0,  $1 \times 10^{-8}$  mbar; 1073 K, 10 min). Afterwards, the sample was flashed to 1073 K in UHV to form the Ir(100)-(5  $\times$  1) reconstruction. We flashed the sample to 873 K in  $\text{O}_2$  atmosphere ( $2 \times 10^{-8}$  mbar) and subsequently cooled it down to room temperature in  $\text{O}_2$  ( $2 \times 10^{-8}$  mbar). This procedure yields the Ir(100)-(2  $\times$  1)-O superstructure, as confirmed by LEED. We prepared epitaxially grown  $\text{Co}_3\text{O}_4(111)$  films by physical vapor deposition (PVD) of Co (Alfa Aesar, 99.95%) onto the Ir(100)-(2  $\times$  1)-O surface in  $\text{O}_2$  ( $8 \times 10^{-6}$  mbar) at 300 K. The Co deposition rate was calibrated by a QCM. In this study, we prepared  $\text{Co}_3\text{O}_4(111)$  films with a thickness of 6 nm. After deposition, the sample was subsequently annealed in  $5 \times 10^{-7}$  mbar  $\text{O}_2$  (523 K, 3 min), in  $5 \times 10^{-8}$  mbar  $\text{O}_2$  (698 K, 7 min), and finally in UHV (698 K, 3 min). Formation of well-ordered  $\text{Co}_3\text{O}_4(111)$  films was confirmed by LEED.

Pt NPs were deposited by PVD from a platinum rod (Alfa Aesar, 99.99%) on the  $\text{Co}_3\text{O}_4(111)$  film in UHV at 300 K. The Pt deposition rate was calibrated by a QCM. The deposition time was adjusted to yield the desired nominal Pt thickness. In this work, we prepared two Pt NPs samples with nominal Pt thicknesses of 1.36 and 0.34 monolayers (ML), corresponding to a Pt atom density of  $2 \times 10^{15}$  and  $5 \times 10^{14} \text{ cm}^{-2}$ , respectively. This yields Pt aggregates with an average size of 2.3 and 1.1 nm, respectively (see previous publications [26, 28] for details). Two oxide samples with equal nominal Pt thickness of 1.4 ML were prepared at the MSB, Elettra Synchrotron in Trieste, Italy. The samples with a nominal Pt thickness of 2.0 and 0.13 ML were prepared at Charles University in Prague.

**2.1.2. Preparation of Pt(111) single crystal.** A Pt(111) single crystal with a surface area of  $78.5 \text{ mm}^2$  (MaTecK, 99.999%, depth of roughness  $<0.01 \mu\text{m}$ , accuracy of orientation  $<0.4^\circ$ ) was used for *in-situ* EC-IRRAS measurements. Before each measurement, the Pt(111) single crystal was annealed for 2 min in the flame of a Bunsen burner and cooled down to room temperature in an atmosphere of Ar (Linde, 6.0) and  $\text{H}_2$  (Linde, 5.0) with a volume ratio of  $\sim 3:1$ . Subsequently, the Pt(111) single crystal was transferred to the IR measuring cell protected by a droplet of degassed ultrapure water (MilliQ Synergy UV,  $18.2 \text{ M}\Omega \text{ cm}$  at  $25^\circ \text{C}$ ,  $\text{TOC} < 5 \text{ ppm}$ ).

## 2.2. Cleaning procedure for the electrochemical equipment

All glass and Teflon equipment as well as all metal wires were cleaned thoroughly to avoid carbonaceous contaminations. All equipment was stored in a solution of NOCHROMIX (Sigma-Aldrich) and sulfuric acid (Merck, EMSURE, 98%) overnight. Before the experiments, all equipment was rinsed with ultrapure water 5 times and boiled in ultrapure water 3 times. We annealed all metal wires used as electrodes in the flame of a Bunsen burner and, subsequently, rinsed them with ultrapure water.

## 2.3. EC-IRRAS measurements

EC-IRRAS measurements were performed using a Fourier transform IR spectrometer with evacuated optics (Bruker Vertex 80v), which is equipped with a dedicated IR setup for electrochemical measurements (Bruker) and a liquid nitrogen cooled mercury cadmium telluride detector. We used a home-built Teflon electrochemical cell with a  $\text{CaF}_2$  hemisphere (Korth, diameter 25 mm) as IR transparent window material. All spectra were acquired under potential control using a commercial potentiostat (Gamry Reference 600). For a detailed description of the setup, we refer to the literature [31]. We used a gold wire (MaTecK, 99.9%) as counter electrode (CE) and a commercial Ag/AgCl (ALS, 3 M NaCl, 0.195  $\text{V}_{\text{NHE}}$ ) electrode as reference electrode (RE). We separated the RE from the measuring cell using a stopcock, which serves as a salt-bridge. The background spectra were recorded at 0.3  $\text{V}_{\text{RHE}}$ , and the potential was subsequently increased to 1.1  $\text{V}_{\text{RHE}}$  with potential steps of 0.1 V. At each potential step, we acquired IR spectra with a resolution of  $2 \text{ cm}^{-1}$  and an acquisition time of 57 s (128 scans) per spectrum. Reference spectra of 2-propanol and acetone were recorded in attenuated total reflection (ATR) geometry using a germanium hemisphere as ATR window.

We used a solution of 0.5 M phosphate buffer as electrolyte, which we prepared from 0.5 M  $\text{Na}_2\text{HPO}_4$  (Merck, Suprapur 99.99%) and 0.5 M NaOH (Sigma Aldrich, 99.99%). The buffer was adjusted to pH 10 using a commercial pH meter (SI Analytics, Lab 870) equipped with a commercial pH electrode (SI Analytics BlueLine 14). To study the oxidation of 2-propanol we prepared a solution of 0.2 M 2-propanol (Sigma Aldrich, 99.999%) in the supporting electrolyte. All solutions were degassed with Ar (Linde, 6.0) for at least 20 min before measurements.

After preparation, the as-prepared samples were transferred out of the UHV chamber into ultrapure water without contact to ambient conditions. Subsequently, the samples were transferred into the EC-IRRAS cell while we protected the surface of the sample with a droplet of ultrapure water. For a more detailed description of the transfer procedure we refer to our previous publications [25, 34].

## 2.4. SR-PES measurements

SR-PES and resonant photoemission spectroscopy (RPES) experiments were performed at the MSB, Elettra synchrotron

light facility in Trieste, Italy. The MSB with a bending magnet source provided synchrotron light in the energy range of 21–1000 eV. The UHV end-station (base pressure  $2 \times 10^{-10}$  mbar) was equipped with an electron energy analyzer (Specs Phoibos 150), a rear view LEED optics, a sputter gun ( $\text{Ar}^+$ ), and a gas inlet system. Two electron-beam evaporators for the deposition of Co and Pt metals were installed.

A specially designed electrochemical cell was connected to the analysis chamber via a buffer chamber and a load lock system. The setup allowed a sample transfer between the electrochemical cell and the analysis chamber without exposure to air. A detailed description of the electrochemical setup can be found in our previous publication [26] and in the supporting information (available online at [stacks.iop.org/JPD/54/164002/mmedia](https://stacks.iop.org/JPD/54/164002/mmedia)). We used a gold wire (Hauer, 99.99%) as CE, a commercial Ag/AgCl electrode (ALS, 3 M NaCl, 0.195  $V_{\text{NHE}}$ ) as RE, and the sample as a working electrode. The sample was immersed into the electrolyte for 3 min at constant potentials between 0.5 and 1.5  $V_{\text{RHE}}$ . The electrochemical treatment and sample transfer were carried out under an Ar atmosphere (SIAD 99.999%). Following the electrochemical treatment, the sample was thoroughly rinsed with ultrapure water and transferred into the analysis chamber (see Supporting Information for details). The corresponding procedure was applied to the electrochemical treatment of two 1.4 ML Pt/ $\text{Co}_3\text{O}_4(111)$  model catalysts in pure electrolyte (0.1 M  $\text{K}_2\text{HPO}_4 + \text{KOH}$ , pH 10) and in 2-propanol solution (0.2 M 2-propanol in 0.1 M  $\text{K}_2\text{HPO}_4 + \text{KOH}$ , pH 10).

Core level spectra were acquired with photon energies of 180 eV (Pt 4f, Ir 4f), 380 eV (C 1s), 650 eV (O 1s), and 930 eV (Co 2p, Ir 4f). The binding energies in the spectra were calibrated with respect to the Fermi level. All spectra were acquired at constant pass energy and at an emission angle of the photoelectrons of  $0^\circ$  with respect to the sample normal. The total spectral resolution was 200 meV ( $h\nu = 180$  eV), 360 meV ( $h\nu = 380$  eV), 650 meV ( $h\nu = 650$  eV), and 1 eV ( $h\nu = 930$  eV). All SR-PES data were processed using the KolXPD fitting software [35]. The spectral components in the Pt 4f spectra were fitted with an asymmetric Doniach-Šunjić function convoluted with a Gaussian profile after subtraction of a Shirley background. The  $\text{Co}^{3+}/\text{Co}^{2+}$  concentration ratios in the  $\text{Co}_3\text{O}_4(111)$  supports were determined by means of the RPES method. Briefly, the method is based on evaluation of the resonant intensities of the valence band features associated with the  $\text{Co}^{3+}$  and  $\text{Co}^{2+}$  cations. The Resonant Enhancement Ratio is proportional to the  $\text{Co}^{3+}/\text{Co}^{2+}$  concentration ratio [36].

### 3. Results and discussion

An overview of the electrocatalysts investigated in this work is given in figure 1. We used a Pt(111) single crystal (figure 1(a)) as a reference system for 2-propanol electrooxidation under conditions identical to those described below for the oxide-based samples. The Pt(111) electrode was prepared by flame annealing and subsequent cooling in reducing atmosphere

[37]. This procedure yields large and well-ordered terraces. All oxide-based samples were prepared by PVD in UHV. In the first step, we analyzed the morphology of the samples by STM. The as-prepared  $\text{Co}_3\text{O}_4(111)$  film (figure 1(b)) consists of flat islands with a diameter between 20 and 60 nm. The surface structure of the  $\text{Co}_3\text{O}_4(111)$  film was determined previously [38, 39]. The film is terminated by  $\text{Co}^{2+}$  ions arranged in a hexagonal unit cell with a  $\text{Co}^{2+}$ – $\text{Co}^{2+}$  ion distance of 5.7 Å. The surface is highly ordered and has a low density of defects (vacancies in the surface layer <1%; adatoms 3%–4%).

PVD of Pt leads to the formation of highly dispersed Pt particles with a relatively narrow size distribution. Particle sizes were estimated based on the particle density obtained from STM and the nominal Pt coverage under the assumption of a hemispherical particle shape. Figure 1(c) shows STM images for a nominal Pt coverage equivalent to 2.0 ML. From the estimated particle density of  $1 \times 10^{13} \text{ cm}^{-2}$ , we calculate an average number of 280 Pt atoms per particle. Assuming a hemispherical shape of the particles, we calculate an average particle size of  $\sim 2.5$  nm in diameter (see figure 1(c)). In the following, we will refer to larger particles with an average size of a few nm as ‘conventional NPs’. In figure 1(d) we show an STM image at lower Pt loading. The nominal Pt coverage is equivalent to 0.13 ML Pt (see figure 1(d)). The particle density is estimated to be  $3.8 \times 10^{13} \text{ cm}^{-2}$ . From these numbers, we calculate an average of 5–6 Pt atoms per aggregate. Formally, the calculation of a particle size using the above approach would yield an average diameter of 0.66 nm. In a more microscopic picture, the Pt particles are very small two-dimensional aggregates, in which nearly all Pt atoms are in contact with the  $\text{Co}_3\text{O}_4$  support. In the following, we will denote aggregates with a formal size around 1 nm and below as ‘ultrasmall particles’. For our studies on the 2-propanol oxidation we prepared both types of model systems, conventional and ultra-small particles, in UHV and transferred the samples into the electrochemical environment without prior exposure to ambient atmosphere.

#### 3.1. Electrooxidation of 2-propanol on Pt(111)

In figure 2(a) we display the ATR spectra of 2-propanol and acetone in the spectral region between 1100 and 2500  $\text{cm}^{-1}$ . The spectra are in good agreement with our previous publication [15]. For 2-propanol, the main bands observed are the bending mode of the  $\text{CH}_3$  group  $\delta_{\text{asym}}(\text{CH}_3)/\delta_{\text{sym}}(\text{CH}_3)$  at 1467  $\text{cm}^{-1}$ , the  $\nu/\delta(\text{C-H})$  stretching/bending mode at 1340  $\text{cm}^{-1}$ , the  $\delta(\text{O-H})$  bending mode at 1308  $\text{cm}^{-1}$ , the  $\nu(\text{C-O})$  stretching mode at 1128  $\text{cm}^{-1}$ , and the  $\nu(\text{C-C})$  stretching modes at 1379, 1368, and 1160  $\text{cm}^{-1}$ . For acetone, the sharp band at 1711  $\text{cm}^{-1}$  is attributed to the CO stretching mode  $\nu(\text{C=O})$ . The broad bands at 1436 and 1420  $\text{cm}^{-1}$  are attributed to the bending modes of the  $\text{CH}_3$  group  $\delta(\text{CH}_3)$ . Bands observed at 1358 and 1220  $\text{cm}^{-1}$  are assigned to the bending mode of the  $\text{CH}_3$  group  $\delta_{\text{sym}}(\text{CH}_3)$  and the stretching mode  $\nu_{\text{asym}}(\text{C-C})$ , respectively [15].

As a reference system, we investigated the electrooxidation of 2-propanol on Pt(111) at pH 10 using EC-IRRAS.

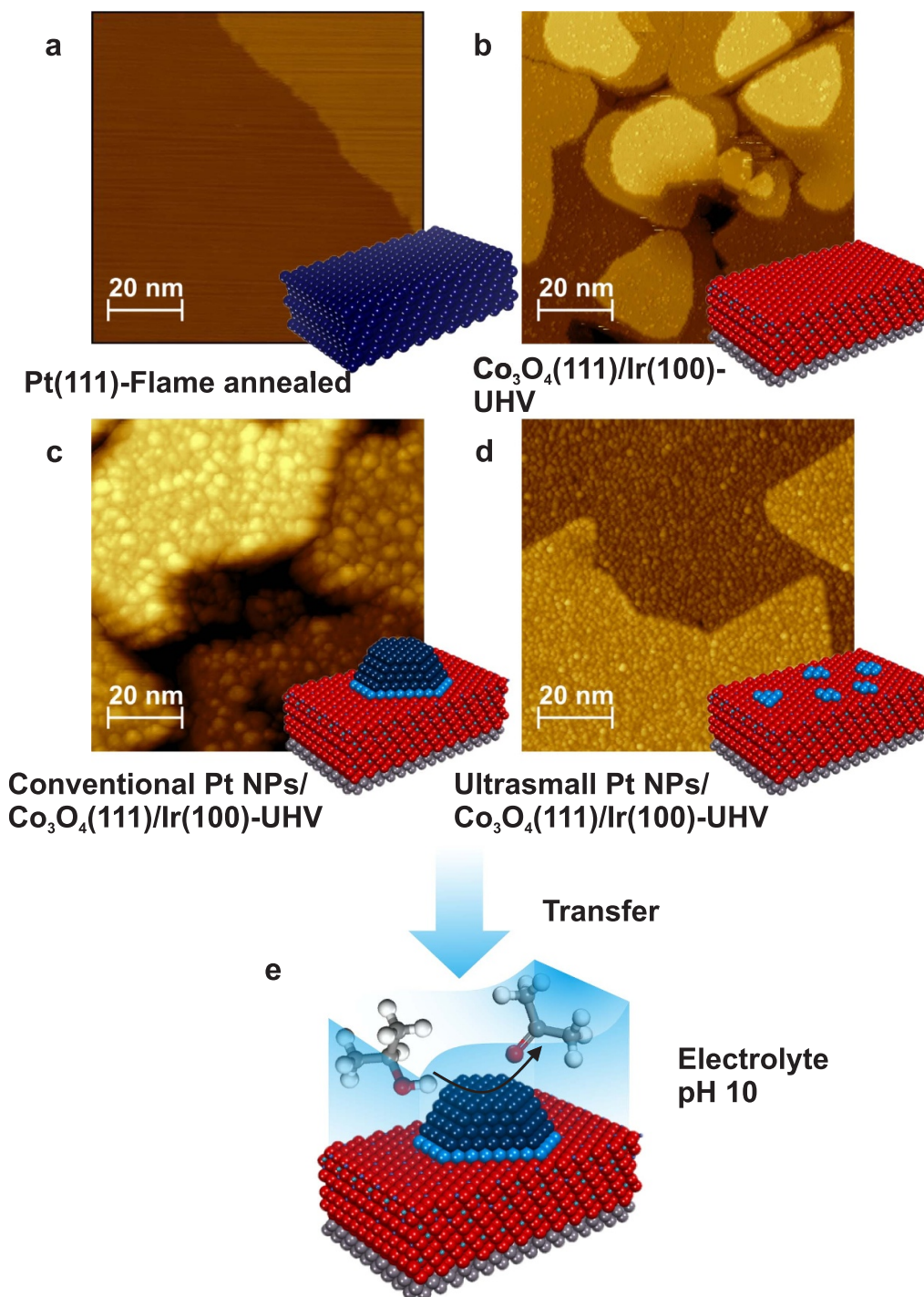


**Figure 1.** (a)–(d) Overview of the electrocatalysts used in this work: (a) STM image of Pt(111); (b) STM image of a well-ordered  $\text{Co}_3\text{O}_4(111)$  film; (c) STM image of conventional Pt NPs on  $\text{Co}_3\text{O}_4(111)$ ; (d) STM image of ultrasmall Pt NPs on  $\text{Co}_3\text{O}_4(111)$ ; (e) schematic representation: transfer of the samples prepared in UHV to electrolyte.

A solution of 0.2 M 2-propanol in 0.5 M phosphate buffer was used in all EC-IRRAS measurements. The resulting IR spectra are displayed as a function of the electrode potential in p-polarization (see figures 2(b) and (c)) and in s-polarization (see figures 2(d) and (e)). All IR spectra are difference spectra with respect to a reference spectrum recorded at 0.3  $V_{\text{RHE}}$ . Subsequently, the potential was increased in steps

of 100 mV from 0.3 to 1.1  $V_{\text{RHE}}$ . In p-polarization, positive bands (pointing upwards) appear at 1467, 1408, 1306, 1166, and 1127  $\text{cm}^{-1}$ . These band positions are in good agreement with our reference spectrum of pure 2-propanol. Small deviations are attributed to solvent effects. Simultaneously, negative bands arise at 1701, 1370, and 1240  $\text{cm}^{-1}$  which are associated with product acetone. Note that in the difference

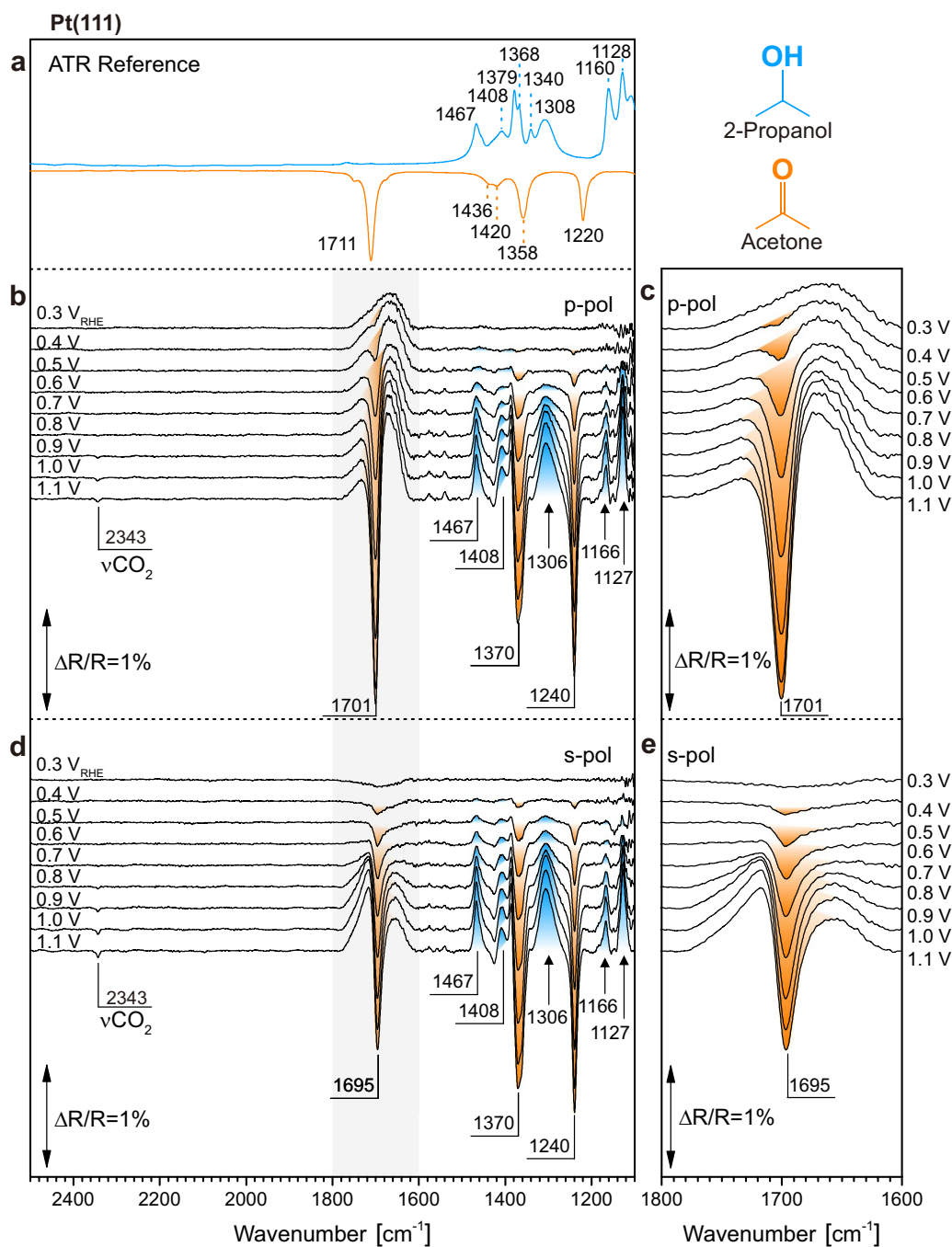


**Figure 2.** Potential-dependent EC-IRRAS spectra obtained during electrooxidation of 2-propanol on Pt(111) at pH 10 (0.2 M 2-propanol in 0.5 M phosphate buffer); (a) ATR IR spectra of pure 2-propanol (blue) and acetone (orange), (b)–(c) IR difference spectra in p-polarization, (d)–(e) IR difference spectra in s-polarization. The reference spectra were acquired at 0.3  $V_{RHE}$ .

spectra positive bands correspond to species which are consumed, whereas negative bands correspond to species which are formed. Therefore, the bands observed indicate the conversion of 2-propanol to acetone. The onset potential for the 2-propanol electrooxidation to acetone is determined to be lower than 0.4  $V_{RHE}$ . This onset potential is in agreement with voltammetric data of the 2-propanol oxidation on Pt electrodes in alkaline environment [40]. Additionally, a weak band at 2343  $cm^{-1}$  appears at 0.8  $V_{RHE}$  and above. This band is attributed to  $CO_2$  in solution formed as a byproduct [16]. Note that

in an alkaline environment we expect the formation of carbonate. The formation of  $CO_2$  bands clearly indicates that there is a pH drop in the thin layer when higher amounts of acetone are formed. Such pH drops are a well-known limitation of EC-IRRAS for reactions which form protons [28] e.g. the 2-propanol oxidation. Note that the pH is almost unaffected at low potentials due to low conversion of 2-propanol to acetone. Still, we minimized the pH drop by using a buffer concentration, which is close to saturation of sodium phosphate. No CO is observed during the 2-propanol electrooxidation,

which is in good agreement with results in an acidic environment [15, 41].

In order to distinguish between the species adsorbed on the electrode surface and the species dissolved in the solution, IR spectra were acquired in s-polarization as well (see figures 2(d) and (e)). Note that in EC-IRRAS on metallic substrates, vibrational bands of adsorbed species are observed in p-polarization only, whereas dissolved species in the electrolyte are visible both in p- and s-polarization due to the metal surface selection rule [42, 43]. Indeed, we observe clear differences between the spectra in p- and s-polarization, which are shown in detail in figures 2(c) and (e), respectively. Within the spectral range, sharp negative  $\nu(\text{C}=\text{O})$  bands associated with acetone are observed in both p- and s-polarization, which overlap with broad positive bands located at  $\sim 1660\text{ cm}^{-1}$ . This broad band is attributed to the  $\delta(\text{HOH})$  bending mode of water. The intensities of the  $\nu(\text{C}=\text{O})$  bands in s-polarization are much weaker than the ones in p-polarization. Additionally, the  $\nu(\text{C}=\text{O})$  bands in s-polarization are red-shifted by  $6\text{ cm}^{-1}$  in comparison to the  $\nu(\text{C}=\text{O})$  bands in p-polarization. Both observations indicate that the formed acetone molecules are partially adsorbed on the electrode surface. In acidic electrolyte, we demonstrated that formed acetone stays mainly adsorbed on Pt surfaces. The adsorbed species partially block the catalyst surface and limit the electrocatalytic activity [15]. We expect that the situation is similar in alkaline environment.

### 3.2. Electrooxidation of 2-propanol on a well-ordered $\text{Co}_3\text{O}_4(111)$ film

In the next step, we investigated the electrooxidation of 2-propanol on  $\text{Co}_3\text{O}_4(111)$  at pH 10. EC-IRRAS measurements were performed following an experimental procedure identical to the one used for Pt(111). In previous studies, we investigated the stability of  $\text{Co}_3\text{O}_4(111)$  films as a function of the electrode potential and pH [27, 34]. We demonstrated that there is an electrochemical stability window at pH 10 between 0.3 and 1.3  $V_{\text{RHE}}$  in which there is no measurable dissolution or restructuring of the surface. Note that the experimental conditions in the present study (phosphate buffer, pH 10, 0.3–1.1  $V_{\text{RHE}}$ ) are all within this stability window. The acquired IR difference spectra in p- and s-polarization are displayed in figures 3(b) and (c), respectively. In strong contrast to the results on Pt(111), for  $\text{Co}_3\text{O}_4(111)$ , we do not detect any bands of 2-propanol and acetone both in p- and in s-polarization. Only broad bands attributed to the  $\delta(\text{HOH})$  bending mode of water are observed in the spectral range of 1800–1500  $\text{cm}^{-1}$ . This observation indicates that the  $\text{Co}_3\text{O}_4(111)$  film is completely inactive towards electrochemical oxidation of 2-propanol under the present electrochemical conditions. 2-Propanol oxidation on  $\text{Co}_3\text{O}_4$  in alkaline environment was previously studied by Sun *et al* using cyclic voltammetry [44]. The authors found a very high onset potential of 1.4  $V_{\text{RHE}}$  [44] indicating a limiting, very high overpotential for the 2-propanol oxidation on  $\text{Co}_3\text{O}_4$ , which is consistent with our observations.

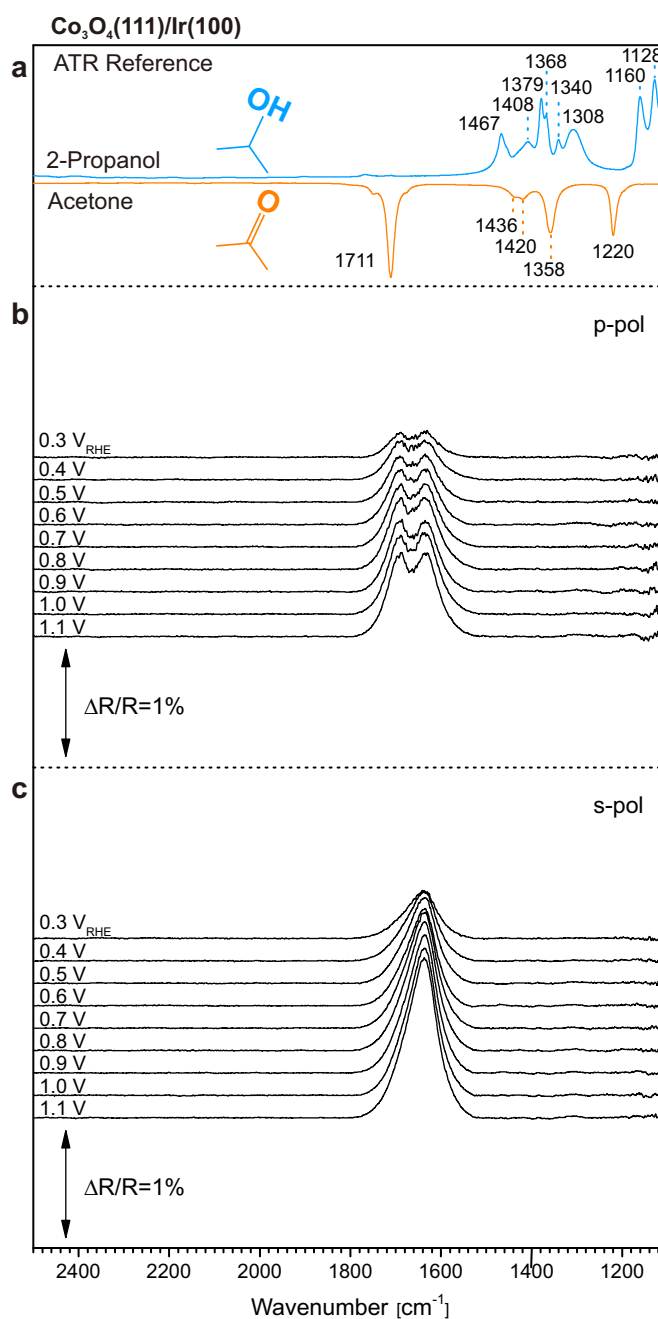


**Figure 3.** Potential-dependent EC-IRRAS spectra obtained during electrooxidation of 2-propanol on well-ordered  $\text{Co}_3\text{O}_4(111)$  film at pH 10 (0.2 M 2-propanol in 0.5 M phosphate buffer); (a) ATR IR spectra of pure 2-propanol (blue) and acetone (orange); (b) IR difference spectra in p-polarization; (c) IR difference spectra in s-polarization. The reference spectra were acquired at 0.3  $V_{\text{RHE}}$ .

### 3.3. Ex-situ emersion SR-PES study of Pt particles supported on $\text{Co}_3\text{O}_4(111)$ films in the absence and presence of 2-propanol

In the next step, we studied the 2-propanol oxidation on Pt/ $\text{Co}_3\text{O}_4(111)$  model catalysts with conventional Pt particles. We used ex-situ emersion SR-PES and RPES to investigate the evolution of the oxidation states of supported Pt NPs and of the  $\text{Co}_3\text{O}_4(111)$  support upon emersion from alkaline

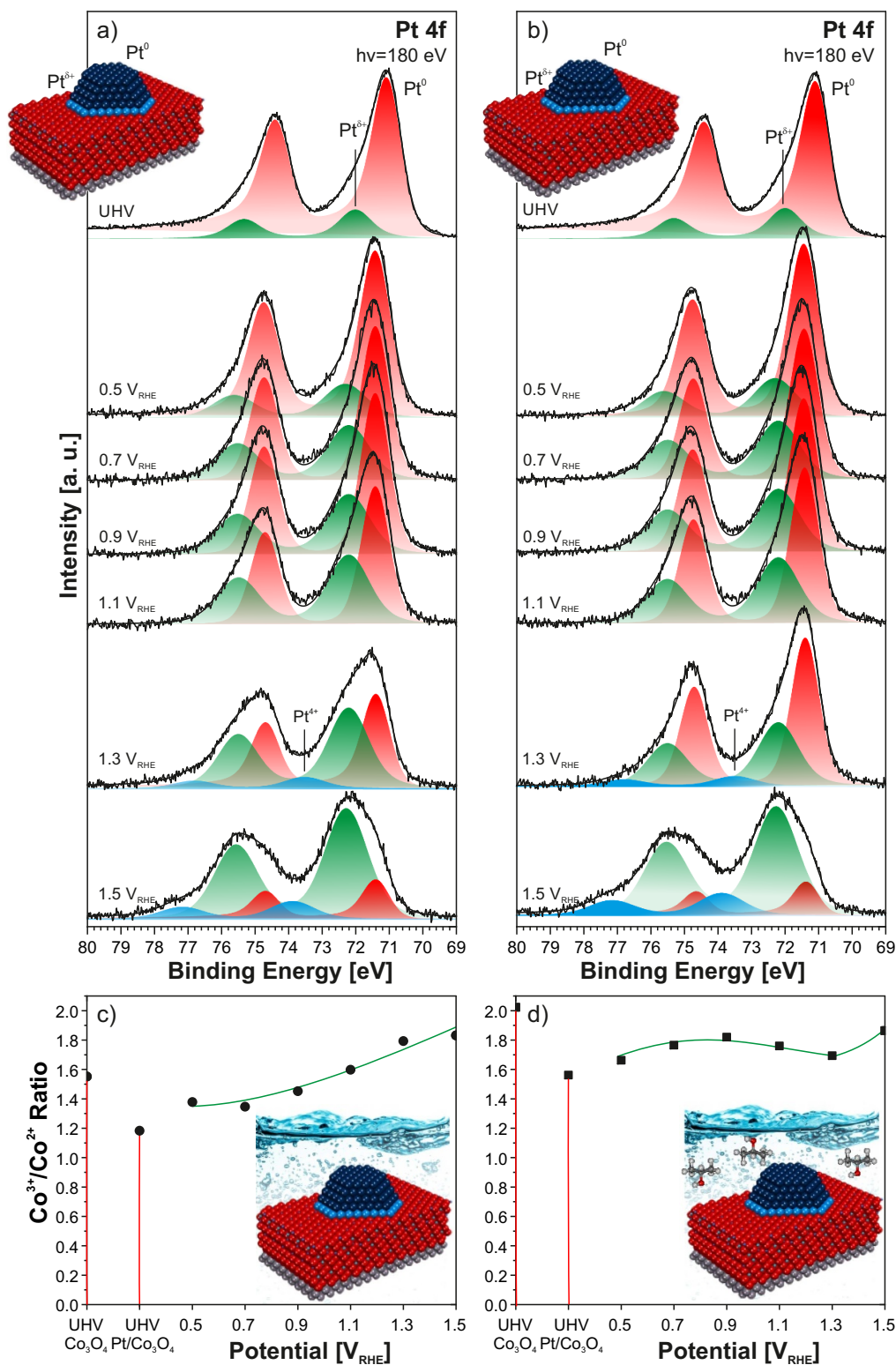


**Figure 4.** Pt 4f spectra (a)–(b) and Co<sup>3+</sup>/Co<sup>2+</sup> ratios (c)–(d) obtained from the Pt/Co<sub>3</sub>O<sub>4</sub>(111)/Ir(100) model catalyst before and after an immersion/emersion cycle from alkaline electrolyte (pH 10) without (a), (c) and with 0.2 M 2-propanol in solution (b), (d). The Pt 4f spectra are normalized to unit area.

electrolyte in the absence and presence of 2-propanol in solution. Toward this aim, two well-defined Pt/Co<sub>3</sub>O<sub>4</sub>(111) model catalysts were prepared with the same nominal Pt coverage and treated under similar conditions. The Pt 4f spectra obtained

from the Pt/Co<sub>3</sub>O<sub>4</sub>(111) model catalysts after preparation and after emersion from electrolytes with potentials between 0.5 and 1.5 V<sub>RHE</sub> are shown in figures 4(a) and (b) for electrolytes without and with 2-propanol present, respectively. The



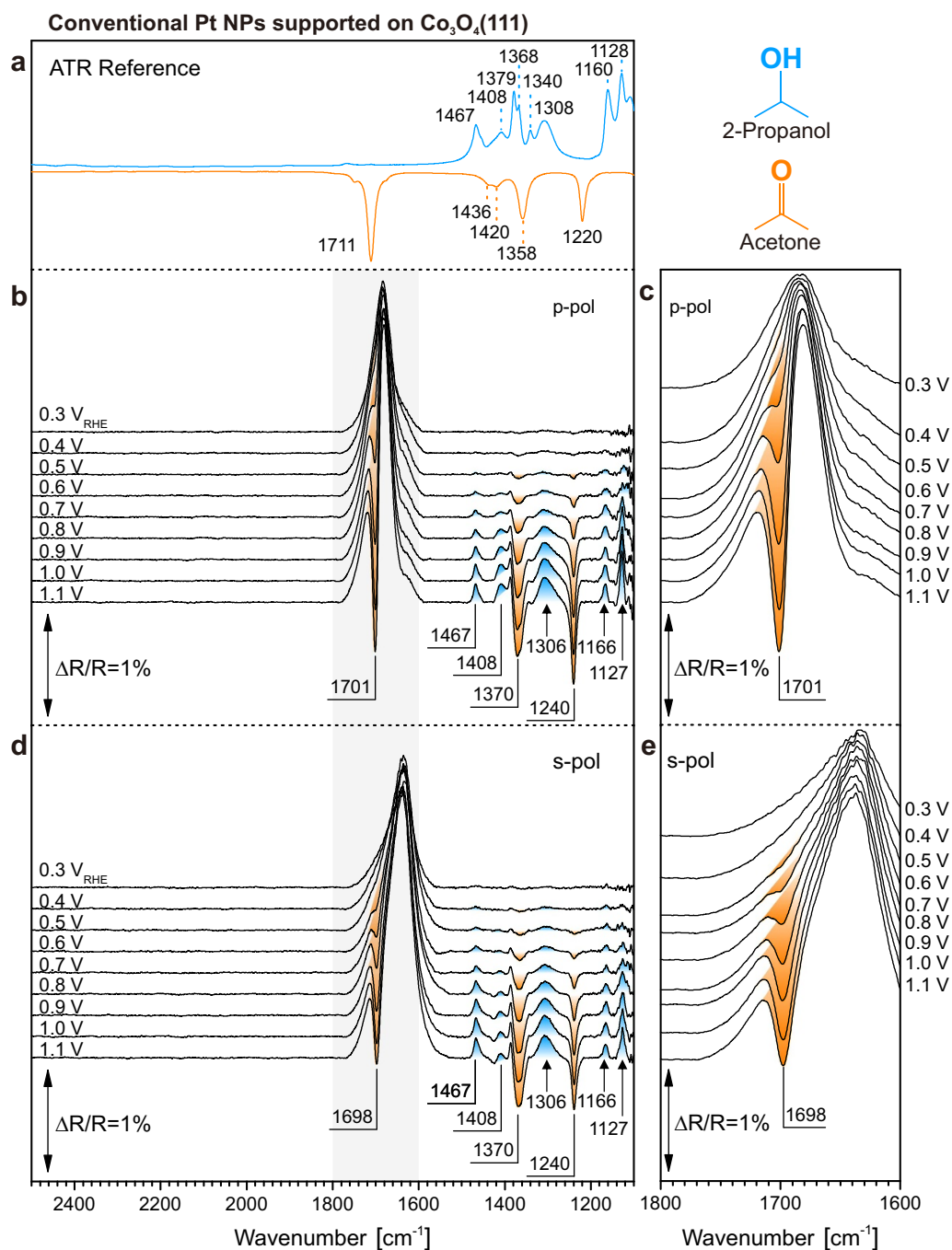


**Figure 5.** Potential-dependent EC-IRRAS spectra obtained during electrooxidation of 2-propanol on conventional Pt NPs at pH 10 (0.2 M 2-propanol in 0.5 M phosphate buffer); (a) ATR IR spectra of pure 2-propanol (blue) and acetone (orange); (b)–(c) IR difference spectra in p-polarization; (d)–(e) IR difference spectra in s-polarization. The reference spectra were acquired at 0.3 V<sub>RHE</sub>.

corresponding Co<sup>3+</sup>/Co<sup>2+</sup> ratios are plotted in figures 4(c) and (d). For a detailed description of the determination of Co<sup>3+</sup>/Co<sup>2+</sup> ratio we refer to the literature [36].

Pt 4f spectra obtained from as-prepared Pt/Co<sub>3</sub>O<sub>4</sub>(111) model catalysts (top spectra) show doublet peaks at 71.0 eV (4f<sub>7/2</sub>) and 72.3 eV (4f<sub>5/2</sub>), which result from metallic Pt<sup>0</sup> and partially oxidized Pt<sup>δ+</sup> species, respectively [25, 29, 30]. Here, the Pt<sup>δ+</sup> species result from the EMSI associated with charge transfer at the Pt/Co<sub>3</sub>O<sub>4</sub>(111) interface [29, 30]. Accordingly, partial reduction of the Co<sub>3</sub>O<sub>4</sub>(111) support

upon Pt deposition is reflected by a decrease of the Co<sup>3+</sup>/Co<sup>2+</sup> ratios on both samples (compare discrete data points in figures 4(c) and (d)).

Following the emersion of the Pt/Co<sub>3</sub>O<sub>4</sub>(111) model catalysts, we observed attenuation of the Pt 4f intensity on both catalysts due to deposition of electrolyte residues and accumulation of adventitious carbon upon emersion and transfer. For a more detailed analysis, we normalized the integrated Pt 4f spectra to unity. In general, we observed minor changes in the Pt 4f spectra upon emersion at 0.5 V<sub>RHE</sub>.

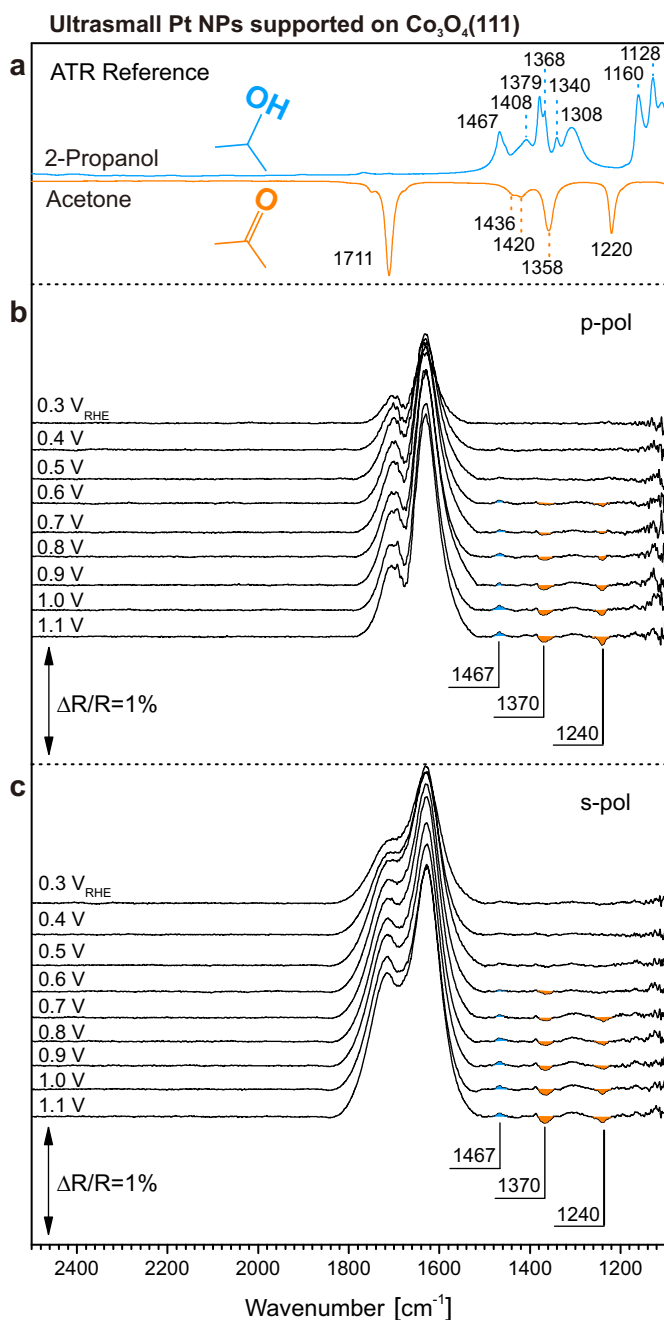


**Figure 6.** Potential-dependent EC-IRRAS spectra obtained during electrooxidation of 2-propanol on ultrasmall Pt NPs at pH 10 (0.2 M 2-propanol in 0.5 M phosphate buffer); (a) ATR IR spectra of pure 2-propanol (blue) and acetone (orange); (b) IR difference spectra in p-polarization; (c) IR difference spectra in s-polarization. The reference spectra were acquired at 0.3  $V_{\text{RHE}}$ .

The  $\text{Pt}^{\delta+}$  contribution increased with respect to  $\text{Pt}^0$ . It should be noted, however, that the  $\text{Pt}^{\delta+}$  contribution overlaps with the  $\text{Pt}^{2+}$  signal from the  $\text{PtO}$  oxide which could be formed upon immersion. The increase of the  $\text{Pt}^{\delta+}/\text{Pt}^{2+}$  contribution is minor between 0.5 and 1.1  $V_{\text{RHE}}$ . At 1.3  $V_{\text{RHE}}$ , however, a strong increase of the  $\text{Pt}^{\delta+}/\text{Pt}^{2+}$  contribution, accompanied by the emergence of a new component at 73.8 eV associated with  $\text{Pt}^{4+}$  states, suggests oxidation of the supported Pt NPs (see figure 4(a)). Primarily, we attribute the effect to

the formation of a surface oxide [26]. Upon increasing the potential to 1.5  $V_{\text{RHE}}$ , the  $\text{Pt}^{\delta+}/\text{Pt}^{2+}$  and the  $\text{Pt}^{4+}$  contributions increase with respect to  $\text{Pt}^0$ . The same behavior was observed earlier on  $\text{Pt}/\text{Co}_3\text{O}_4(111)$  [26].

Comparing the Pt 4f data obtained from the  $\text{Pt}/\text{Co}_3\text{O}_4(111)$  model catalysts in the presence and in the absence of 2-propanol in solution, we observed that the spectra are very similar in the potential range between 0.5 and 1.1  $V_{\text{RHE}}$ . At 1.3  $V_{\text{RHE}}$ , however, we observed weaker oxidation of the supported Pt NPs in the presence of 2-propanol (see figure 4(b)). At 1.5  $V_{\text{RHE}}$ , strong oxidation occurred again even in the presence of 2-propanol. Interestingly, we observed a gradual increase of the  $\text{Co}^{3+}/\text{Co}^{2+}$  concentration ratio after immersion into pure electrolyte between 0.5 and 1.5  $V_{\text{RHE}}$  (see figure 4(c)). This trend seems to be weaker in the presence of 2-propanol. In particular, the  $\text{Co}^{3+}/\text{Co}^{2+}$  concentration ratio hardly changes between 0.5 and 1.3  $V_{\text{RHE}}$  and increases only at the potential step to 1.5  $V_{\text{RHE}}$ . These observations suggest that the fast 2-propanol oxidation to some extent prevents the oxidation of the  $\text{Pt}/\text{Co}_3\text{O}_4(111)$  catalysts.

#### 3.4. Electrooxidation of 2-propanol on conventional Pt NPs

Next, we investigated the conventional Pt NPs supported on  $\text{Co}_3\text{O}_4(111)$  during electrooxidation of 2-propanol by EC-IRRAS. Here, we applied the same procedures as previously described for  $\text{Pt}(111)$  and  $\text{Co}_3\text{O}_4(111)$ . The corresponding spectra are shown in figure 5. In p-polarization, we observe negative bands at 1700, 1370 and 1240  $\text{cm}^{-1}$ , which are associated with the formation of acetone (see figures 5(b) and (c)). At the same time, positive bands are observed at 1467, 1408, 1306, 1166 and 1127  $\text{cm}^{-1}$ , which are associated with the consumption of 2-propanol. The band positions are in perfect agreement with those observed on  $\text{Pt}(111)$  and the band intensities increase with increasing electrode potential. This observation suggests that the conventional Pt NPs supported on  $\text{Co}_3\text{O}_4$  are active towards the conversion of 2-propanol to acetone under alkaline conditions. The onset potential of 2-propanol conversion is found to be 0.5  $V_{\text{RHE}}$ , which is  $\sim 0.1$  V higher than for the  $\text{Pt}(111)$  surface. Notably, no  $\text{CO}_2$  is observed during the whole process of 2-propanol electrooxidation, indicating that the pH drop is small and the pH in the thin layer remains in the alkaline region. Note, however, that bands of carbonate (expected at 1366 and 1270  $\text{cm}^{-1}$ ) [29] would overlap with the intense bands of 2-propanol and acetone. Therefore, we cannot exclude the formation of small amounts of carbonate. No adsorbed CO was detected, similarly to what was observed on the  $\text{Pt}(111)$  surface. The difference spectra obtained in s-polarization are displayed in figures 5(d) and (e). Direct comparison of spectra obtained in p- and s-polarization shows distinct differences. As discussed above, the negative  $\nu(\text{C}=\text{O})$  bands overlap with the positive  $\delta(\text{HOH})$  bending mode of water. Still, we observe that the band intensity in s-polarization is weaker compared to the band in p-polarization and the band position is slightly shifted. These differences indicate that the product acetone is partially adsorbed on the Pt NPs surface, resulting in partial blocking of the active sites.

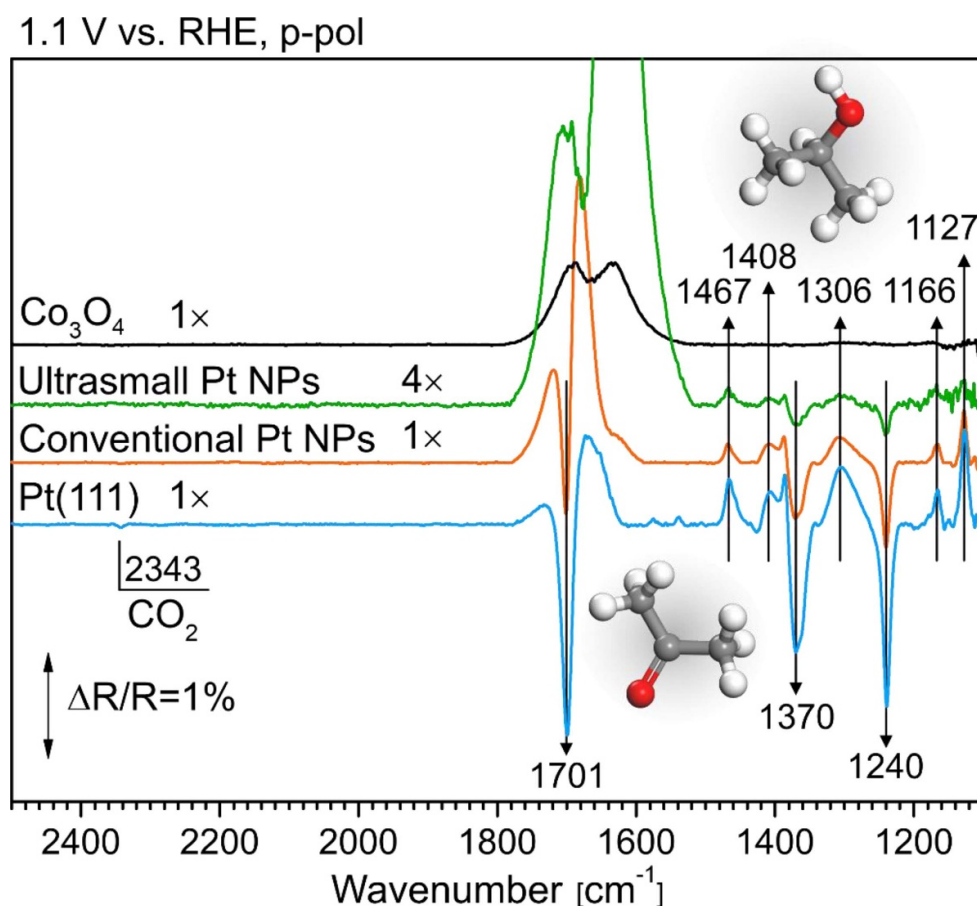


**Figure 7.** Comparison of the EC-IRRAS spectra obtained during electrooxidation of 2-propanol on different electrocatalysts at an electrode potential of 1.1  $V_{\text{RHE}}$  in p-polarization. The reference spectra were acquired at 0.3  $V_{\text{RHE}}$ .

### 3.5. Electrooxidation of 2-propanol on ultrasmall Pt NPs

In order to investigate the size effect on the activity of Pt NPs, we performed EC-IRRAS measurements during 2-propanol electrooxidation on ultrasmall Pt particles. The corresponding IR spectra are shown in figure 6 as a function of electrode potential. In contrast to the intense bands observed for the conventional NPs, only weak features are observed for the ultrasmall Pt NPs. The positive band at  $1467\text{ cm}^{-1}$  is attributed to the  $\delta_{\text{asym}}(\text{CH}_3)/\delta_{\text{sym}}(\text{CH}_3)$  vibrations of consumed 2-propanol, the negative bands at  $1370$  and  $1240\text{ cm}^{-1}$  are attributed to the  $\delta_{\text{sym}}(\text{CH}_3)/\nu_{\text{asym}}(\text{C}-\text{C})$  and  $\nu_{\text{asym}}(\text{C}-\text{C})$  vibrations of acetone. The most intense band of acetone, which is associated with  $\nu(\text{C}=\text{O})$ , overlaps with the  $\delta(\text{HOH})$  bending mode of water between  $1800$  and  $1600\text{ cm}^{-1}$  (see spectra of the pristine  $\text{Co}_3\text{O}_4(111)$  film in figure 3). Therefore, this band could not be observed. The low intensity of the bands indicates that only minor amounts of acetone are formed and the activity of  $\text{Pt}/\text{Co}_3\text{O}_4(111)$  is low. In our previous study, the oxidation states of Pt NPs were investigated as a function of particle size [26]. We showed that in contrast to the conventional Pt NPs, the ultrasmall Pt NPs mainly consist of partially oxidized  $\text{Pt}^{\delta+}$  species with small fractions of  $\text{Pt}^{4+}$  and  $\text{Pt}^0$  present only. We conclude that the oxidized Pt species is largely inactive towards 2-propanol oxidation. The small

residual activity observed for  $\text{Pt}/\text{Co}_3\text{O}_4(111)$  is attributed to the presence of small amounts of metallic Pt.

A direct comparison of the EC-IRRAS spectra from  $\text{Pt}(111)$ ,  $\text{Co}_3\text{O}_4(111)$  film, conventional Pt NPs, and ultrasmall Pt NPs is provided in figure 7. All spectra were obtained at  $1.1\text{ V}_{\text{RHE}}$  in 2-propanol solution (0.2 M 2-propanol in 0.5 M phosphate buffer at pH 10) with p-polarized IR light. For the  $\text{Pt}(111)$  reference, we observe intense bands below  $1800\text{ cm}^{-1}$  associated with 2-propanol and acetone. An additional small band at  $2343\text{ cm}^{-1}$  is attributed to  $\text{CO}_2$  in solution. The observed bands indicate that  $\text{Pt}(111)$  is highly active for conversion of 2-propanol to acetone (the large concentration of protons released during the reaction even shifts the pH in the thin layer of electrolyte into the acidic region). For the  $\text{Co}_3\text{O}_4(111)$  film, we do not observe bands of 2-propanol and acetone, indicating that this system is completely inactive under the present electrochemical conditions. In contrast, strong bands of 2-propanol and acetone are observed for the model electrocatalyst comprised of conventional Pt NPs on  $\text{Co}_3\text{O}_4(111)$ . The band positions are in excellent agreement with those observed on  $\text{Pt}(111)$ . Notably, no  $\text{CO}_2$  is detected in this system, indicating that the buffer concentration is sufficient to stabilize the pH in the alkaline region. For ultrasmall Pt NPs supported on  $\text{Co}_3\text{O}_4(111)$ , only weak bands are detected. All active electrocatalysts studied oxidize

2-propanol to acetone with high selectivity and no CO was formed on any of these catalysts.

Our findings show that there is a pronounced size effect of the oxide supported Pt particles with a strongly decreased activity of small Pt aggregates. We attribute the low residual activity to a small fraction of active Pt<sup>0</sup> species, while the majority of Pt is present as inactive Pt<sup>δ+</sup>. In previous work we demonstrated, however, that the EMSI can be beneficial to stabilize the Pt NPs against sintering [30]. Thus the Pt<sup>δ+</sup> species may help to maintain a high activity of electrocatalysts at higher Pt loading in spite of the fact that the Pt<sup>δ+</sup> species themselves are not active. Consequently, we expect a rather complex size dependent effect of the EMSI on activity. While the stability and, thereby, also the activity of Pt particles in the nanometer range may be enhanced by EMSI, the activity decreases rapidly when going to ultrasmall Pt particles which are easily oxidized.

#### 4. Conclusion

We have investigated the electrooxidation of 2-propanol on atomically defined Pt/Co<sub>3</sub>O<sub>4</sub> model electrocatalysts with different Pt particle sizes in an alkaline environment (phosphate buffer, pH 10). The model catalysts were prepared in UHV and their structure and morphology were characterized by STM. Freshly prepared model electrocatalysts were transferred into the electrochemical environment without exposure to ambient atmosphere. The 2-propanol oxidation was studied by means of EC-IRRAS and SR-PES. Additionally, we performed reference experiments under identical conditions on Pt(111) and pristine Co<sub>3</sub>O<sub>4</sub>(111). From our findings, we conclude the following:

- (a) *Activity of Pt(111) single crystals and plain Co<sub>3</sub>O<sub>4</sub>(111)*: 2-Propanol is oxidized on Pt(111) in alkaline media (pH 10, phosphate buffer) to acetone with high selectivity. The onset potential of the reaction is below 0.4 V<sub>RHE</sub>. The product acetone is partially adsorbed on the electrode surface poisoning the electrocatalyst. No adsorbed CO is formed during the reaction. In sharp contrast, Co<sub>3</sub>O<sub>4</sub>(111) is inactive towards 2-propanol oxidation between 0.3 and 1.1 V<sub>RHE</sub>.
- (b) *Characterization of conventional Pt NPs on Co<sub>3</sub>O<sub>4</sub>(111) in the electrochemical environment*: Conventional Pt NPs on Co<sub>3</sub>O<sub>4</sub>(111) consist of metallic Pt<sup>0</sup> and partially oxidized Pt<sup>δ+</sup> species located at the metal–support interface both after preparation (UHV) as well as between 0.5 and 1.1 V<sub>RHE</sub>. Surface Pt oxide species (Pt<sup>2+</sup> and Pt<sup>4+</sup>) are formed above 1.1 V<sub>RHE</sub>. In general, the presence of 2-propanol has little effect on the oxidation state of Pt but can slightly attenuate Pt oxidation during the electrocatalytic reaction.
- (c) *2-Propanol oxidation with conventional NPs on Co<sub>3</sub>O<sub>4</sub>(111)*: Conventional NPs on Co<sub>3</sub>O<sub>4</sub>(111), for which metallic Pt<sup>0</sup> is the dominating species, are highly active towards 2-propanol oxidation under alkaline conditions (pH 10, phosphate buffer). The onset potential is

~0.5 V<sub>RHE</sub>. Acetone is formed with high selectivity and no CO was detected as byproduct. Similarly to Pt(111), acetone partially adsorbs on the Pt NPs and leads to partial blocking of the active sites.

- (d) *2-Propanol oxidation with ultrasmall particles on Co<sub>3</sub>O<sub>4</sub>(111)*: Ultrasmall particles, which consist mainly of partially oxidized Pt<sup>δ+</sup>, have a very low activity for the 2-propanol oxidation. We attribute a low residual activity of the ultrasmall particles to traces of Pt<sup>0</sup> that are still present on the surface.

Our results demonstrate that Pt/Co<sub>3</sub>O<sub>4</sub>(111) is a highly active and stable electrocatalyst for selective oxidation of 2-propanol. However, there is an intricate interplay between particle size effects and EMSI. While the EMSI is beneficial for the stability of the Pt NPs, the electronically modified Pt<sup>δ+</sup> species do not show catalytic activity.

#### Acknowledgments

The authors acknowledge financial support by the Deutsche Forschungsgemeinschaft (DFG) (Project 431733372, 322419553) and additional support by the DFG (Research Unit FOR 1878 ‘Functional Molecular Structures on Complex Oxide Surfaces’, Projects 214951840, CH 1763/5-1). The authors acknowledge financial support by the German Federal Ministry of Education and Research (BMBF, Project Combined Infrared and X-Ray Analytics of Energy Materials, CIXenergy 05K19WE1) and by the Bavarian Ministry of Economic Affairs, Regional Development and Energy. Further financial support is given by the Helmholtz Institute Erlangen-Nürnberg for Renewable Energy and the DFG within the Cluster of Excellence ‘Engineering of Advanced Materials’ (Project EXC 315) (Bridge Funding). The authors acknowledge the support of the Czech Science Foundation (project GAČR 20-11688J). The authors acknowledge the CERIC-ERIC Consortium for the access to experimental facilities and financial support. The authors further acknowledge the Czech Ministry of Education (LM2018116). L F would like to thank the Grant Agency of the Charles University (project GAUK 262120) for support. We acknowledge the support provided by the China Scholarship Council (CSC) during a visit of T Y at the Friedrich-Alexander Universität Erlangen-Nürnberg.

#### ORCID iDs

Tomáš Skála  <https://orcid.org/0000-0003-2909-9422>  
 Kevin C Prince  <https://orcid.org/0000-0002-5416-7354>  
 Viktor Johánek  <https://orcid.org/0000-0002-8833-5870>  
 Josef Mysliveček  <https://orcid.org/0000-0003-2305-2711>  
 Olaf Brummel  <https://orcid.org/0000-0001-5968-0774>

#### References

- [1] Niaz S, Manzoor T and Pandith A H 2015 Hydrogen storage: materials, methods and perspectives *Renew. Sustain. Energy Rev.* **50** 457–69

- [2] Edwards P P, Kuznetsov V L, David W I and Brandon N P 2008 Hydrogen and fuel cells: towards a sustainable energy future *Energy Policy* **36** 4356–62
- [3] Teichmann D, Arlt W, Wasserscheid P and Freymann R 2011 A future energy supply based on liquid organic hydrogen carriers (LOHC) *Energy Environ. Sci.* **4** 2767–73
- [4] Teichmann D, Arlt W and Wasserscheid P 2012 Liquid organic hydrogen carriers as an efficient vector for the transport and storage of renewable energy *Int. J. Hydrog. Energy* **37** 18118–32
- [5] Amende M et al 2014 Size and structure effects controlling the stability of the liquid organic hydrogen carrier dodecahydro-N-ethylcarbazole during dehydrogenation over Pt model catalysts *J. Phys. Chem. Lett.* **5** 1498–504
- [6] Amende M et al 2014 Model catalytic studies of liquid organic hydrogen carriers: dehydrogenation and decomposition mechanisms of dodecahydro-N-ethylcarbazole on Pt (111) *ACS Catal.* **4** 657–65
- [7] Gleichweit C et al 2013 Dehydrogenation of dodecahydro-N-ethylcarbazole on Pt (111) *ChemSusChem* **6** 974–7
- [8] Sobota M et al 2011 Dehydrogenation of dodecahydro-N-ethylcarbazole on Pd/Al<sub>2</sub>O<sub>3</sub> model catalysts *Chem. Eur. J.* **17** 11542–52
- [9] Brückner N, Obesser K, Bösmann A, Teichmann D, Arlt W, Dungs J and Wasserscheid P 2014 Evaluation of industrially applied heat-transfer fluids as liquid organic hydrogen carrier systems *ChemSusChem* **7** 229–35
- [10] Sievi G et al 2019 Towards an efficient liquid organic hydrogen carrier fuel cell concept *Energy Environ. Sci.* **12** 2305–14
- [11] Kormanyos A, Speck F D, Mayrhofer K J and Cherevko S 2020 Influence of fuels and pH on the dissolution stability of bifunctional PtRu/C alloy electrocatalysts *ACS Catal.* **10** 10858–70
- [12] Hauenstein P, Seeberger D, Wasserscheid P and Thiele S 2020 High performance direct organic fuel cell using the acetone/isopropanol liquid organic hydrogen carrier system *Electrochem. Commun.* **118** 106786
- [13] Khanipour P, Speck F D, Mangoufis-Giasin I, Mayrhofer K J, Cherevko S and Katsounaros I 2020 Electrochemical oxidation of isopropanol on platinum–ruthenium nanoparticles studied with real-time product and dissolution analytics *ACS Appl. Mater. Interfaces* **12** 33670–8
- [14] Xu M, Yu J, Song Y, Ran R, Wang W and Shao Z 2020 Advances in ceramic thin films fabricated by pulsed laser deposition for intermediate-temperature solid oxide fuel cells *Energy Fuels* **34** 10568–82
- [15] Waidhas F, Haschke S, Khanipour P, Fromm L, Görling A, Bachmann J, Katsounaros I, Mayrhofer K J, Brummel O and Libuda J 2020 Secondary alcohols as rechargeable electrofuels: electrooxidation of 2-propanol at Pt electrodes *ACS Catal.* **10** 6831–42
- [16] Pastor E, González S and Arvia A J 1995 Electroreactivity of isopropanol on platinum in acids studied by DEMS and FTIRS *J. Electroanal. Chem.* **395** 233–42
- [17] Otomo J, Li X, Kobayashi T, Wen C-J, Nagamoto H and Takahashi H 2004 AC-impedance spectroscopy of anodic reactions with adsorbed intermediates: electro-oxidations of 2-propanol and methanol on carbon-supported Pt catalyst *J. Electroanal. Chem.* **573** 99–109
- [18] Santasalo A, Vidal-Iglesias F, Solla-Gullón J, Berná A, Kallio T and Feliu J 2009 Electrooxidation of methanol and 2-propanol mixtures at platinum single crystal electrodes *Electrochim. Acta* **54** 6576–83
- [19] Liu J, Ye J, Xu C and Tong Y 2008 Electro-oxidation of methanol, 1-propanol and 2-propanol on Pt and Pd in alkaline medium *J. Power Sources* **177** 67–70
- [20] Markiewicz M E and Bergens S H 2010 A liquid electrolyte alkaline direct 2-propanol fuel cell *J. Power Sources* **195** 7196–201
- [21] Antolini E and Gonzalez E 2010 Alkaline direct alcohol fuel cells *J. Power Sources* **195** 3431–50
- [22] Xu C, Tian Z, Shen P and Jiang S P 2008 Oxide (CeO<sub>2</sub>, NiO, Co<sub>3</sub>O<sub>4</sub> and Mn<sub>3</sub>O<sub>4</sub>)-promoted Pd/C electrocatalysts for alcohol electrooxidation in alkaline media *Electrochim. Acta* **53** 2610–8
- [23] Kolb D M 2001 Electrochemical surface science *Angew. Chem. Int. Ed.* **40** 1162–81
- [24] Niluis N, Wallis T M and Ho W 2003 From single atoms to one-dimensional solids: artificial gold chains on NiAl (110) *Japan. J. Appl. Phys.* **42** 4790
- [25] Faisal F et al 2018 Electrifying model catalysts for understanding electrocatalytic reactions in liquid electrolytes *Nat. Mater.* **17** 592–8
- [26] Bertram M et al 2020 Cobalt oxide-supported Pt electrocatalysts: intimate correlation between particle size, electronic metal-support interaction and stability *J. Phys. Chem. Lett.* **11** 8365–71
- [27] Brummel O et al 2019 Redox behavior of Pt/Co<sub>3</sub>O<sub>4</sub>(111) model electrocatalyst studied by x-ray photoelectron spectroscopy coupled with an electrochemical cell *J. Phys. Chem. C* **123** 8746–58
- [28] Faisal F and et al 2018 Atomically-defined model catalysts in ultrahigh vacuum and in liquid electrolytes: particle size-dependent Co adsorption on Pt nanoparticles on ordered Co<sub>3</sub>O<sub>4</sub> (111) films *Phys. Chem. Chem. Phys.* **20** 23702–16
- [29] Faisal F et al 2018 Electrocatalysis with atomically defined model systems: metal-support interactions between Pt nanoparticles and Co<sub>3</sub>O<sub>4</sub> (111) under ultrahigh vacuum and in liquid electrolytes *J. Phys. Chem. C* **122** 20787–99
- [30] Lykhach Y et al 2018 Interplay between the metal-support interaction and stability in Pt/Co<sub>3</sub>O<sub>4</sub> (111) model catalysts *J. Mater. Chem. A* **6** 23078–86
- [31] Faisal F, Bertram M, Stumm C, Waidhas F, Brummel O and Libuda J 2018 Preparation of complex model electrocatalysts in ultra-high vacuum and transfer into the electrolyte for electrochemical IR spectroscopy and other techniques *Rev. Sci. Instrum.* **89** 114101
- [32] Meyer W, Biedermann K, Gubo M, Hammer L and Heinz K 2008 Surface structure of polar Co<sub>3</sub>O<sub>4</sub> (111) films grown epitaxially on Ir (100)-(1 × 1) *J. Phys.: Condens. Matter* **20** 265011
- [33] Biedermann K, Gubo M, Hammer L and Heinz K 2009 Phases and phase transitions of hexagonal cobalt oxide films on Ir (100)-(1 × 1) *J. Phys.: Condens. Matter* **21** 185003
- [34] Faisal F, Bertram M, Stumm C, Cherevko S, Geiger S, Kasian O, Lykhach Y, Lytken O, Mayrhofer K J and Brummel O 2018 Atomically defined Co<sub>3</sub>O<sub>4</sub> (111) thin films prepared in ultrahigh vacuum: stability under electrochemical conditions *J. Phys. Chem. C* **122** 7236–48
- [35] Libra J Kolxpd: spectroscopy data measurement and processing (available at: [www.Kolibrik.Net/Science/Kolxpd/](http://www.Kolibrik.Net/Science/Kolxpd/)) (Accessed 15 September 2017)
- [36] Lykhach Y et al 2019 Quantitative analysis of the oxidation state of cobalt oxides by resonant photoemission spectroscopy *J. Phys. Chem. Lett.* **10** 6129–36
- [37] Kibler L 2000 Preparation and characterization of noble metal single crystal electrodes (available at: [www.uni-ulm.de/echem/ekat/downloadpage.html](http://www.uni-ulm.de/echem/ekat/downloadpage.html))
- [38] Heinz K and Hammer L 2013 Epitaxial cobalt oxide films on Ir (100)—the importance of crystallographic analyses *J. Phys.: Condens. Matter* **25** 173001
- [39] Behm R J, Buchner F, Eckardt M, Böhler T, Kim J, Gerlach J and Schnaidt J 2020 ORR and OER on Ni-modified Co<sub>3</sub>O<sub>4</sub> (111) cathodes for Zn-air batteries—a combined surface

- science and electrochemical model study *ChemSusChem* **13** 3199–211
- [40] Liu J, Ye J, Xu C, Jiang S P and Tong Y 2008 Electro-oxidation of methanol, 1-propanol and 2-propanol on Pt and Pd in alkaline medium *J. Power Sources* **177** 67–70
- [41] Sun S-G and Lin Y 1996 *In situ* FTIR spectroscopic investigations of reaction mechanism of isopropanol oxidation on platinum single crystal electrodes *Electrochim. Acta* **41** 693–700
- [42] Iwasita T and Nart F 1997 *In situ* infrared spectroscopy at electrochemical interfaces *Prog. Surf. Sci.* **55** 271–340
- [43] Hoffmann F M 1983 Infrared reflection-absorption spectroscopy of adsorbed molecules *Surf. Sci. Rep.* **3** 107–92
- [44] Sun S, Sun L, Xi S, Du Y, Prathap M A, Wang Z, Zhang Q, Fisher A and Xu Z J 2017 Electrochemical oxidation of C3 saturated alcohols on Co<sub>3</sub>O<sub>4</sub> in alkaline *Electrochim. Acta* **228** 183–94